The jamming transition and the marginally jammed solid

Andrea J. Liu[1] and Sidney R. Nagel[2]

[1]*Department of Physics and Astronomy, University of Pennsylvania, Philadelphia, PA 19104;* [2]*The James Franck Institute, The University of Chicago, Chicago, IL 60637*

Key Words jamming, glass transition, colloids, granular materials, foams, emulsions

Abstract When a system jams it undergoes a transition from a flowing to a rigid state. Despite this important change in the dynamics, the internal structure of the system remains disordered in the solid as well as the fluid phase. In this way jamming is very different from crystallization, the other common way in which a fluid solidifies. Jamming is a paradigm for thinking about how many different types of fluids – from molecular liquids to macroscopic granular matter – develop rigidity. Here we review recent work on the jamming transition. We start with perhaps the simplest model of frictionless spheres interacting via repulsive finite-range forces at zero temperature. In this highly-idealized case, the transition has aspects of both first- and second-order transitions. From studies of the normal modes of vibration for the marginally jammed solid, new physics has emerged for how a material can be rigid without having the elastic properties of a normal solid. We first survey the simulation data and theoretical arguments that have been proposed to understand this behavior. We then review work that has systematically gone beyond the ideal model to see whether the scenario developed there is more generally applicable.

This includes work that examines the effect of non-spherical particles, friction and temperature on the excitations and the dynamics. We briefly touch on recent laboratory experiments that have begun to make contact with simulations and theory.

CONTENTS

1 INTRODUCTION

William Butler Yeats bemoaned that " Things fall apart; the centre cannot hold; Mere anarchy is loosed upon the world...". Equally calamitous is that things get stuck and often seemingly at the worst possible moment–they lose the ability to flow so that no further rearrangement is possible. This can occur as particles get wedged tightly together in a pipe on a factory floor or as molasses refuses to pour from a container as the temperature drops in winter. Of course, falling apart and getting stuck are just approaching from opposite directions this catastrophic transition in the dynamics, known as the jamming transition. Our goal here is to review some progress that has been made in seeing if the concept of a jamming transition has a more general applicability (in the purely physical realm!) than had previously been realized and whether it can unite our understanding of different ways in which a flowing material or liquid can gain rigidity.

A liquid with low viscosity solidifies into a glass when the temperature is lowered; a flowing foam becomes rigid when the applied stress is lowered; a colloidal suspension loses the ability to flow when the density is increased. In each of these cases, a different control parameter is varied to bring the system into the rigid phase yet the structure does not change appreciably at the transition. Both phases are amorphous and no structural "order parameter has been identified to tell the two apart. A common framework could prove useful for revealing connections between these seemingly disparate phenomena.

A theory for jamming phenomena must account for the extraordinary increase in relaxation times associated with the "transition". However, this dramatic slow down itself poses experimental problems and makes it difficult to study the very phenomena being investigated. There is no (first-order) jump as in

crystallization nor is it possible to approach very closely the point at which the relaxation times might appear to diverge. The laboratory transition is determined by kinetics: the definition of the glass-transition temperature, T_g, depends on the choice of an arbitrary time (or equivalently, viscosity) scale (1, 2). If an experiment is carried out more slowly, a supercooled liquid remains fluid to a (slightly) lower temperature so that T_g decreases. Similar behavior occurs in the onset of rigidity in a driven system such as a foam: more patient measurements produce lower values of the yield stress, Σ_y. Such transitions are therefore not sharp (1); experiments, always done on a laboratory time scale, cannot produce a unique value for either the glass-transition temperature or the yield stress. Even with fourteen decades of dynamic range in frequency, experiments have not been able to verify or refute the possibility that there is a underlying sharp finite-temperature transition.

One important advance in the study of jamming is that, at least for one admittedly idealized model described below, there is a well-defined transition where an order parameter can be defined. In this simplified case the physics is beginning to be put on a firm foundation. This physics is *not* merely an extension of previously known results but contains new elements. It is presently a subject of considerable controversy whether this jamming transition, interesting as it is, will be relevant to more realistic systems and whether it has the explanatory power to deal with the complexities of glass formation. However, a solid understanding of the physics in one region of phase space is an advance that offers the hope that this understanding can be enlarged at least to the region around it.

Our review of jamming starts by considering the "spherical cow" model of ideal spheres at zero temperature and zero shear stress. These frictionless spheres

interact with repulsive pair potentials that vanish at a well-defined distance that defines their diameter. Because we restrict ourselves initially to zero temperature, the system is always in mechanical equilibrium where the forces on all particles balance. At low enough packing fraction, the particles are free to push each other apart so that there are no overlaps. In this case, the particles are free to move in response to any stress on the system - it behaves as a fluid. At higher packing fraction, the particles are forced to overlap and the system is jammed - any infinitesimal force will be resisted by the force network between the spheres. At a critical value of the packing fraction the system is precariously perched between a liquid and a solid state. This sharp transition itself is unusual in that it exhibits both a discontinuity, as in a first-order transition, and power-law scaling, as in an ordinary critical point. Moreover, the properties of the marginally-jammed solid, just above the transition, differ from those of ordinary elastic solids.

This particular transition can be placed on a so-called "jamming phase diagram" (3), as shown in Fig. 1. The advantage of looking at it in the context of such a diagram is that it allows one to see how this transition might relate to more realistic materials such as granular matter or glasses. The phase diagram has three axes specifying the relevant control parameters: T (temperature), $1/\phi$ (the inverse density or packing fraction of particles), and Σ (shear stress). The region near the origin (in green) is jammed and the region far from the origin represents material that can flow. The lines in the $(T - 1/\phi)$ and $(1/\phi - \Sigma)$ planes represent the generic dynamical glass transition and yield stress, respectively. Those curves are drawn to show that as the density is increased, one normally expects that a system will become more rigid. The shape of the jamming surface will vary from system to system; the purpose of this diagram is to

identify the important control parameters for jamming and to see how different systems might relate to one another. We note that the control parameters are not necessarily thermodynamic variables (*i.e.*, the shear stress can drive the system into a flowing state) yet they do control the rigidity of the system. Note that the jamming surface is not sharply defined in the dynamics as discussed above. The transition for ideal sphere systems is denoted by "J" in Fig. 1 and lies at zero temperature and shear stress at a density ϕ_c at which the spheres just begin to have unavoidable overlap.

In this review, we take the point of view that by studying in detail this transition and the properties of the marginally-jammed solid, we can obtain a deeper understanding of the nature of jamming transitions and of amorphous solids in general. Particular attention will be paid to the normal modes of vibration in the jammed solid. If the zero-temperature solid is to lose rigidity due to an infinitesimal decrease in packing fraction, it must do so by creating at least one soft mode (*i.e.*, a mode with zero frequency). This is how a solid under shear stress fails (4, 5). But in that case, the failure produces another solid and not a fluid with very different properties. We therefore expect that the complete loss of rigidity at J should be more catastrophic and should not be reflected in the behavior of just a single soft mode. The low-frequency modes of the solid should display a characteristic signature as the jamming/unjamming transition is approached.

It turns out that this signature is indeed dramatic. The shape of the vibrational spectrum and nature of the low-frequency modes at the unjamming threshold are completely different from those ordinary solids. This result has implications for the behavior of glasses at low temperature as well as for other amorphous

systems. As the temperature is raised evenly slightly above zero, the lowest frequency modes will be the dominant excitations. Thus they not only control how the marginal solid falls apart due to a small decrease in density, but also how it responds to a small increase in temperature or applied stress.

Section II summarizes the properties of the transition and of the marginally-jammed solid. The remainder of the review is organized around different ways of perturbing the system around point J. In Section III, we discuss work on extending the results to nonzero temperatures and shear stresses, respectively. This is the first step towards exploring the connection between the transition at point J and the glass transition or the development of a yield stress in ideal spheres. In Section IV, we discuss generalizations of the ideal sphere model to explore the extent to which the behavior of ideal spheres is applicable to more realistic systems. Finally, in Section V we discuss open questions that are the subject of active research.

2 Properties of the zero-temperature jamming transition

Numerical simulations suggest that the zero-temperature jamming transition of ideal spheres, point J in Fig. 1, is a special transition with aspects of both first- and second-order behavior and with multiple diverging and vanishing length scales associated with its approach. Despite its unusual nature, this transition still controls many of the properties of the system in its vicinity in the manner of an ordinary critical point.

The analysis that follows is centered around ideal spheres or discs in two and three dimensions, which interact via the following pairwise potentials:

$$V(r_{ij}) = \frac{\epsilon}{\alpha}(1 - \frac{r_{ij}}{\sigma_{ij}})^{\alpha}, \tag{1}$$

where $\sigma_{ij} = (\sigma_i + \sigma_j)/2$ is the average of the diameters of particles i and j. The case $\alpha = 2$ corresponds to harmonic repulsions between particles while $\alpha = 5/2$ corresponds to Hertzian repulsions in three dimensions and $\alpha = 0$ corresponds to hard-sphere repulsions.

2.1 Isostaticity and scaling near point J

The order parameter that characterizes the transition is Z, the average number of overlaps a particle has with its neighbors. At low density, $Z = 0$ since if particles are not forced to be in contact, they will push each other apart leaving no overlapping particles. In order to have any overlap, a particle must be held in place by neighbors on all sides, so overlapping particles must span the entire system. In consequence, Z must jump discontinuously from $Z = 0$ to a nonzero value, Z_c at the transition packing fraction, ϕ_c. For frictionless spheres, Z_c turns out to be the minimum possible value needed for mechanical stability (7–10), due to the following argument. A mechanically stable system must have force balance on every particle so that for N spheres in the connected backbone in d dimensions, the number of equations that must be satisfied by the inter-particle forces is Nd. According to Maxwell's criterion for rigidity (6) the number of inter-particle forces, $NZ/2$, must be at least the number of equations (assuming no degeneracies). This leads to the condition $Z \geq 2d$. For particles with finite-ranged repulsions at the onset of jamming, however, the amount of overlap between particles in contact must also vanish. This introduces $NZ/2$ equations that must be satisfied by the dN particle coordinates. Thus, at the jamming transition, one also has the condition $d \geq Z/2$. The two conditions can only be satisfied by $Z_c = 2d$.

When the system is compressed above the transition, the coordination number Z increases above Z_c. The excess number of contacts scales as (9, 11, 12)

$$Z - Z_c \sim \Delta\phi^{\beta \approx 1/2}, \tag{2}$$

The existence of isostaticity at the transition implies a diverging length scale (10,13,14). Consider a system that is compressed to a packing fraction $\Delta\phi$ above the transition. Such a system has an excess of $Z - Z_c \sim \Delta\phi^{1/2}$ contacts beyond those needed for mechanical stability. If a chunk of material of size ℓ is cut from the d-dimensional system, there will be ℓ^{d-1} boundary contacts missing. If the total number of contacts in the chunk, $N_{\rm tot}$, is below the isostatic value, $N_{\rm iso} = NZ_c/2$, there will be zero-frequency modes (floppy or soft modes). The number of soft modes is therefore given by the difference between the contacts cut at the boundary of the chunk and the extra contacts in the bulk of the chunk:

$$N_{\rm soft} \approx c_1 \ell^{d-1} - c_2 (Z - Z_c) \ell^d, \tag{3}$$

where c_1 and c_2 are constants that depend on the geometry of the chunk. The "cutting length" $\ell^\star$ is the size of the chunk at which $N_{\rm soft}$ vanishes, so that the excess number of contacts in the bulk is equal to the number of missing contacts at the perimeter:

$$\ell^\star \sim \Delta\phi^{-\nu \approx -1/2}. \tag{4}$$

Below $\ell^\star$, the system looks isostatic but above $\ell^\star$, the system is over-coordinated and should behave as a normal elastic solid. This length scale was observed in simulations probing fluctuations in the response of a packing to a point force or to a small inflation of a single particle, as shown in Fig 2.

Above ϕ_c, the elastic moduli vary as power laws with increasing packing fraction, $\Delta\phi = \phi - \phi_c$ (9, 11, 12). The pressure, p, the bulk modulus, B and the

shear modulus, G all vanish in the unjammed regime at $\phi < \phi_c$. The elastic constants are conveniently expressed in terms of the effective elastic constant for the interaction, $k_{\rm eff}$, given by the second derivative of the pair interaction, V'', which scales as $k_{\rm eff} \sim \Delta\phi^{\alpha-2}$. The moduli scale as $B \sim k_{\rm eff}$ and $G \sim k_{\rm eff}\Delta\phi^{0.5}$. Note that the ratio

$$\frac{G}{B} \sim \Delta\phi^{\gamma \approx 1/2} \tag{5}$$

does not depend on the interaction potential and vanishes at the transition.

The behavior of the coordination number $Z - Z_c$ in Eq. 2 is reflected in the pair-correlation function, $g(r)$. At the transition, there is divergent first peak in $g(r)$ due to a delta-function at contact with amplitude Z_c; this arises from the Z_c neighbors per particle that are just in contact there (15). As the system approaches the transition, the overlap distance, or the width of the first peak in $g(r)$ on the small-r side, ℓ_w, vanishes as (15)

$$\ell_w \sim \Delta\phi, \tag{6}$$

while the height of the first peak diverges (15) as $g_1 \sim \Delta\phi^{-1.0}$. In addition, the pair-correlation function near the jamming transition has the functional form $g(r) \propto \sqrt{r-\sigma}$ for r above but close to the sphere diameter, σ (16). When integrated, this yields Eq. 2 (12). Similar results were observed for hard spheres approaching ϕ_c from below (17).

There is a vanishing frequency scale associated with the vibrational spectrum. Consider the chunk of size ℓ cut from the system at the isostatic transition. As argued earlier, each of the ℓ^{d-1} bonds that is cut at the perimeter of this chunk yields a floppy mode. If these modes are assumed to be extended, we can use each one to create a trial vibrational mode for the chunk when it is compressed to some $\Delta\phi$ above the transition. Each trial mode is assumed to be a floppy mode

distorted by a plane wave that satisfies the boundary condition that the mode amplitude vanishes at the boundary of the chunk where the bonds were cut. This distortion leads to an energy cost of $\mathcal{O}(1/\ell^2)$, so that the corresponding mode has frequency $\omega \sim \sqrt{k_{\rm eff}/m}\ \sqrt{1/\ell^2} \sim \sqrt{k_{\rm eff}/m}\ \mathcal{O}(1/\ell)$. For a chunk compressed to $\Delta\phi$, the onset frequency of "anomalous" modes corresponding to floppy modes shifted upwards in frequency upon compression should be determined by the cutting length, $\ell^\star \sim \Delta\phi^{-0.5}$, as defined in Eq. 4; this frequency then scales as

$$\omega^* \sim \sqrt{\frac{k_{\rm eff}}{m}}\ \Delta\phi^{z \approx 1/2}, \tag{7}$$

If we assume that the modes are plane-wave-like below ω^*, so that they obey the dispersion relation $\omega = ck$, where c is the speed of sound and k is the wavevector, this yields two length scales $\ell \propto 1/k$, corresponding to the longitudinal and transverse sound speeds, determined by the bulk and shear moduli, respectively, with $\ell^\star \approx c_\ell/\omega^* \sim \Delta\phi^{-\nu=-1/2}$ consistent with the cutting length of Eq. 4. This length scale has also been observed in the dispersion relation (18, 19). At frequencies above ω^*, many wavevectors contribute to the anomalous modes, but the lowest wavevectors that contribute are of order $1/\ell^*$.

There is also a new length scale (18)

$$\ell^\dagger \approx c_t/\omega^* \sim \Delta\phi^{-\nu^\dagger \approx -1/4}, \tag{8}$$

which also marks the mean-free path of vibrations at the crossover between weak and strong scattering at $\omega^\star$ (19–21).

There appears to be another diverging length scale whose connection to the length scales introduced above is not understood. The finite-size shift of the position of the jamming transition, ϕ_c, yields a length scale that apparently diverges as $|\phi - \phi_c|^{-0.7}$ in both 2- and 3- dimensions (9). The same exponent

shows up in simulations in which a hard disk is pushed through a packing below ϕ_c (22). Finally, the same exponent has been observed for correlations of the transverse velocity on athermal, slowly-sheared sphere packings near the jamming transition, (23) but only for certain models of the dynamics (JJ Remmers, unpublished). It is not known whether the exponent is really different from 1/2 or not.

In summary, we have a transition consistent with a discontinuity in the coordination number and a diverging length scale. Such as a transition is known as a random first order transition (24). The apparently rational values of the exponents for the jamming transition and the fact that the numerically-calculated exponents are the same in two and three dimensions suggest that the transition is mean-field-like. An Imry-Ma-type argument due to Wyart (10) suggests that the upper critical dimension of the jamming transition should be two. If one includes disorder in the coordination number that could lead to additional soft modes, the number of soft modes in a cut chunk of size ℓ in Eq. 3 is modified:

$$N_{\rm soft} = c_1\ell^{d-1} - c_2(Z - Z_c)\ell^d + c_3\delta Z L^{d/2} \tag{9}$$

where δZ characterizes the amount of disorder. Evidently, disorder does not affect the transition if $d/2 \leq d-1$, or equivalently, if $d \geq 2$.

To understand the interplay of isostaticity and disorder, it is useful to study isostatic systems with no disorder. A recent analysis (25) considers periodic isostatic lattices in $d = 2$ stabilized by next-nearest-neighbor bonds. By tuning the strength of the next-nearest-neighbor bonds to zero, the systems are taken towards an isostatic structural transition. One can identify a cutting length, $\ell^\star$, and crossover frequency, $\omega^\star$, that scale as expected. However, the ratio G/B varies among systems, periodic or disordered, exhibiting isostatic transitions (25–

27). In the square lattice with randomly added next-nearest-neighbor bonds (27), G/B varies as $(Z - Z_c)^2$, not $Z - Z_c$ as for the jamming transition (Eq. 5 and 2), while for a randomly diluted network, G/B is constant with $Z - Z_c$ (26). This suggests that isostaticity alone is not enough to determine the universality class of the structural transition.

The particular behavior displayed by the jamming transition—a discontinuity and subsequent power-law increase with $\beta \approx 1/2$ in the number of interacting neighbors, a divergent susceptibility (or inverse ratio of shear to bulk modulus) with $\gamma \approx 1/2$ and two diverging length scales with exponents $\nu \approx 1/2$ and $\nu^\dagger \approx 1/4$—is rare but has been seen in several models. Remarkably, all of these models correspond to ones that have been proposed for the glass transition or that capture glassy dynamics (24, 28–33), in the mean-field limit. Another class of models known as k-core percolation (34) and its variants, called "jamming percolation," (35–40) also displays the same behavior in the mean-field limit as the jamming transition (40). These models yield some insight into the connection of one class of models with glassy dynamics, namely kinetically-constrained spin models (31), to the jamming transition. In k-core percolation, which maps onto kinetically-constrained spin models (41, 42), sites are populated randomly with probability p. The "k-core" is the set of occupied sites with at least k occupied neighbors, each of which has at least k neighbors, and so on. In jammed packings, on the other hand, each particle in the connected cluster must be locally stable with at least $d+1$ neighbors to hold it in place; each of these neighbors must have at least $d+1$ neighbors, and so on. This analogy between k-core percolation and jamming is not an exact mapping, because the former model is a scalar model, not a vector one. As a result, the global constraint that there must be at least $2d$

neighbors per particle on average is not satisfied in k-core percolation because it is a scalar model, not a vector one. Consequently, the two models do not exhibit the same behavior in $d = 2$ (38, 39), but are apparently similar enough to have the same behavior in the mean-field limit.

Finally, there have been several suggestions for a "statistical mechanics" of stable packings, starting with Oakeshott and Edwards (43–47). This approach suggests a field theoretical analysis of the packings (46) which, when combined with empirical arguments, leads to a proposed phenomenological mean field theory for the jamming transition (48).

2.2 Location of point J

Each mechanically stable configuration corresponds to a local minimum in the potential-energy landscape. For ideal spheres, the properties of different minima are remarkably similar so that to a large extent, the properties of a minimum are dictated by its energy. Now consider a given local minimum with some energy V. As the system is decompressed, V decreases and eventually reaches $V = 0$. At this density, ϕ_c, the state corresponding to the energy minimum has reached its jamming threshold and is isostatic.

Different minima or mechanically stable configurations can have different jamming thresholds, ϕ_c. The width of the distribution of jamming thresholds vanishes in the infinite system-size limit, so that nearly all distinct states jam at the same density (9,12). This density is $\phi_J \approx 0.84$ for two-dimensional bidisperse packings of disks, and $\phi_J \approx 0.64$ for three-dimensional packings of monodisperse spheres, close to random close-packing density, $\phi_{\rm rcp}$.

However (9,12), we know (49) that there is a small tail of states at higher and

lower densities. Because there is a distribution of jamming thresholds even in the thermodynamic limit, different protocols can yield different results by weighting states differently. For example, equilibrating a sample at a finite temperature before quenching to $T = 0$ can lead to an increase in its jamming threshold density above ϕ_c. Depending on the preparation history of the system, the jamming transition of an ensemble can therefore occur over a range of densities (50, 51). Such a range in the case in which the densest close-packed state is assumed to be disordered is shown in Fig. 7.

2.3 Harmonic properties of the marginally-jammed solid at T=0

A defining characteristic of the vibrational spectrum of elastic solids is that at sufficiently low frequency, the vibrations are plane wave sound modes. This behavior gives rise to the familiar Debye scaling of the vibrational density of states with frequency, $D(\omega) \sim \omega^{d-1}$, for a solid in d dimensions. One of the most striking features of marginally-jammed sphere packings at $\phi = \phi_c^+$ is that they violate this Debye law. Instead, $D(\omega)$ is simply a plateau (**?**) down to zero frequency in both $d = 2$ and $d = 3$. As shown in Fig. 3, the plateau persists upon compression but only down to a low-frequency cutoff, $\omega^\star$, that increases with $\Delta\phi$ as in Eq. 7 (18). We note that in amorphous solids, modes in excess of the Debye prediction for plane-waves arise at a frequency called the boson peak frequency; thus, our system has a boson peak frequency of $\omega^\star$.

These modes arise from soft modes at the jamming transition. The variational calculation (10, 13, 14) outlined above Eq. 7 describes the frequency shift of the soft modes upon compression. The number of soft modes created by the cutting a chunk of size ℓ scales as $N_\ell \sim \ell^{d-1}$. If one assumes that the modes upon

compression can be viewed as plane-wave distortions of the soft modes, which vanish at the edges of the boundary, the resulting modes are shifted upwards to frequencies up to $\omega_\ell \sim 1/\ell$, as argued above Eq. 7. The total number of modes in the chunk scales as ℓ^d. Thus, the density of states must satisfy

$$\int_0^{\omega_\ell} d\omega D(\omega) \approx \frac{N_\ell}{\ell^d} \sim \frac{1}{\ell} \sim \omega_\ell. \tag{10}$$

Clearly, this is satisfied if $D(\omega) \sim$ const, independent of ω. This argument suggests that the observed constant behavior of the density of states should persist down to zero frequency at the jamming transition (Fig. 3).

Another question concerns the structure of the normal modes, shown in Fig. 4. In the vicinity of $\omega^\star$ the modes are highly heterogeneous and resonant, with large displacements of a few particles superimposed on a plane-wave-like background. The modes become progressively more heterogeneous and "quasi-localized" as the frequency is lowered (Fig. 5(a) and Fig. 4(b)). There is no appreciable difference in the magnitude of the participation ratio for the lowest-frequency modes at the different compressions, suggesting that quasi-localized modes exist even at the jamming threshold. Similar modes have been observed in other disordered solids (52–59). Above $\omega^\star$, the modes become more extended (Fig. 4(c)) with contributions from a very broad range of wavevectors (19, 60). These are the anomalous modes, presumed to originate from the soft modes at the isostatic jamming transition. At high frequency, the modes are highly localized (Fig. 4(d)), as expected.

The nature of the modes affects their contribution to the thermal conductivity, κ, as quantified by the energy diffusivity, $d(\omega)$. The quantity $d(\omega)$ is defined as follows. A wave packet peaked at ω and localized at r spreads over time and can be characterized by $d(\omega)$, given by the square of the width of the wave packet

divided by time at long times. (In a weakly-scattering three-dimensional system, $d(\omega) = c\ell(\omega)/3$, where c is the sound speed and $\ell(\omega)$ is the phonon mean-free path.)

For sphere packings, the diffusivity was calculated using the Kubo approach (19, 20). At low frequencies, the diffusivity behaves as for weakly-scattered plane waves. Above a crossover frequency that scales as $\omega^\star$, $d(\omega)$ is nearly frequency independent, consistent with theoretical expectations (10, 19, 21). Such a regime, postulated to exist in glasses to explain the temperature dependence of the thermal conductivity (61), thus arises from properties of the jamming transition (19, 20). The scaling of the crossover from weakly-scattered plane waves to strong scattering can be understood by assuming continuity of the mean-free path in conjunction with the scaling laws for the shear and bulk moduli (19, 20).

Recently, dynamical effective medium theory (62,63) has been used to study the dynamics of a square lattice with randomly-placed next-nearest-neighbor springs (27) and random isotropic off-lattice systems near the isostatic limit (21). Both calculations yield a characteristic frequency $\omega^* \sim Z - Z_c$ above which the density of states $D(\omega)$ and the diffusivity $d(\omega)$ exhibit a plateau. In the isotropic case (21), both the zero-frequency bulk and shear moduli vanish as $Z - Z_c$ in agreement with static effective medium calculations for rigidity percolation (64) so that their ratio is constant, unlike Eq. 5. In addition, both $D(\omega)$ and $d(\omega)$ exhibit a plateau above a frequency $\omega^* \sim \Delta Z$, in agreement with numerical results (12, 18–20). If the starting point is a periodic isostatic system(27), the frequency-dependent shear modulus, $C_{44}(\omega)$, satisfies the scaling relation $C_{44}(\omega)/C_{44}(0) = h(\omega/\omega^*)$. This model also yields $l^* \sim (\Delta z)^{-1}$ in agreement with the cutting arguments discussed above Eq. 4 (10, 13, 14).

2.4 Anharmonic properties of the marginally-jammed solid at T=0

In order to consider how a solid disintegrates and loses rigidity, either at high temperature or under a mechanical load, we must push beyond the harmonic approximation and consider the anharmonic response of the solid. It has not been generally appreciated that on approaching the unjamming transition, the barriers between nearby configurations shrink to zero so that anharmonic effects will also diverge.

The existence of low-frequency quasi-localized modes (Fig. 5(a)), suggests that the structural stability of jammed solids might be very different from that of ordinary crystals, according to the following argument. Because such modes have a somewhat localized character, the same energy input into one of them, as compared to an extended mode, would drive some particles to have much larger amplitude of oscillation. In addition, the relative displacement between a particle and its neighbor will also be very large because the high displacements contain very high wavevector components.

Application of shear stress can push a mode frequency downwards until it reaches zero (5). At that point the system must rearrange into a new stable configuration. Compressive stress can have the same effect. For crystals, the shift of frequency with compression is typically small and negative. For disordered sphere packings, however, the shift is highly negative (65) for the low-frequency, low-participation ratio modes shown in Fig. 5(a), indicating that such modes are highly unstable to compression. Another measure of the anharmonicity is how far a given mode can be excited (leaving all the others alone) before the system goes unstable (65). Fig. 5(b) shows that the low-frequency quasi-localized modes

are the most anharmonic.

3 EFFECT OF TEMPERATURE AND STRESS ON POINT J

The progress on understanding the jamming transition discussed in Sec. II was possible because properties can be studied cleanly at zero temperature. Each mechanically-stable configuration corresponds to a metastable energy minimum whose properties can be studied simply by using energy minimization. Working at $T = 0$ is appropriate for granular systems and foams, where the energy for even small rearrangements of the configuration is many orders of magnitude greater than the thermal energy at room temperature. However, for molecular glasses, temperature is obviously relevant. In this section, we review work that has been done to connect the zero-temperature jamming transition at point J to phenomena at nonzero temperature.

3.1 Effect of temperature on length scales near point J

The jamming transition at point J is marked by diverging length scales and a vanishing length scale, the overlap distance. One strategy for understanding behavior at nonzero temperature is to track these lengths and watch their evolution as temperature T increases from zero. The effect of T on the overlap distance has been studied numerically and experimentally (66). It has been shown that $\ell_w \ \phi - \phi_v(T)$, consistent with the scaling of Eq. 6 at zero temperature. Indeed, recent results suggest that above $\phi_v(T)$ the elastic moduli also scale with $\phi - \phi_v(T)$ as they do at zero temperature (67). This suggests that the behavior at $\phi_v(T)$ is a vestige of the jamming transition at $T = 0$. The vestige has been observed experimentally on two-dimensional bidisperse systems of NIPA particles by Zhang,

et al. (66).

3.2 Sphere systems in thermal equilibrium

While the zero-temperature plane in the jamming phase diagram (Fig. 1) can be studied by energy minimization, the unjammed region can be studied numerically by standard methods such as molecular dynamics simulations. Here we focus on equilibrium properties of the repulsive sphere systems characterized by the potentials of Eq. 1, approaching the jamming surface from high temperature. Such systems exhibit typical glass-transition behavior, with a relaxation time that increases with decreasing T at fixed pressure, p. For colloidal systems such as hard-sphere suspensions, on the other hand, p or ϕ is typically varied at fixed T. Recent molecular dynamics simulations (68) show that in the limit of low pressure, the relaxation time, τ, along many different trajectories in the $T-\phi$ plane, can be scaled onto a single master plot as a function of the ratio T/p. Ref. (68) argues that this collapse should hold for all repulsive potentials that vanish at a finite distance, as long as $p\sigma^d/\epsilon$ is small, where σ is the particle diameter and ϵ is the scale of the interaction energy. However, the low-pressure limit for soft spheres is equivalent to the hard-sphere limit, where $\epsilon \to \infty$. In this limit, the data collapse shows that the glass transition and the colloidal glass transition are actually the same phenomenon.

Point J for soft spheres corresponds to the double limit $p\sigma^d/\epsilon \to 0$, $T/p\sigma^d \to 0$. This also corresponds to the infinite-pressure limit ($p\sigma^d/T \to \infty$) of hard spheres. This equivalence explains why the properties of the maximally-random jammed state of hard spheres (69) are identical to the properties of soft spheres at point J. It also tells us that we can learn about the effect of temperature on point J by

studying hard spheres just below the jamming transition.

Brito and Wyart (70–72) proposed an important conceptual extension of the results for athermal soft-sphere systems above point J to those of hard-sphere systems below point J. The analogy is valid at times long compared to the collision time of the hard spheres but short compared to the rearrangement time. Although each particle has many neighbors, it does not necessarily collide with all of them. Following earlier work for granular materials (73), one can define a contact network of particles that experience many collisions with each other. The coordination is Z_c at the transition and increases as Eq. 2 below ϕ_c (70). Each particle in this network has an average position and fluctuates around this average position as it explores its free volume. From the free-volume entropy, one can obtain a dynamical matrix for the system. Thus, the vibrational behavior discussed in Sec. II.B-C has been extended to hard spheres below the jamming transition (71, 72).

3.3 Effect of stress on the jamming transition

The rheology near point J was first studied by Olsson and Teitel (23) using the bubble model introduced by Durian (11, 74) for modelling foams. They found that the viscosity, $\eta \equiv \Sigma/\dot{\gamma}$, where Σ is the steady-state shear stress and $\dot{\gamma}$ is the shear rate, exhibits scaling collapse onto two branches, one above and the other below the critical jamming density, ϕ_c (see Fig. 6). This data collapse suggests that the jamming transition is indeed critical.

4 BEYOND THE IDEAL SPHERE MODEL

Up to now, we have focused on the behavior of packings of frictionless spheres interacting via purely repulsive, finite-ranged potentials. Clearly, no system in nature is so ideal and it is important to understand the extent to which the results apply to more realistic systems. To this end, several groups have explored generalizations such as non-spherical particle shapes, friction, and long-ranged interactions, including attractions. Here we will show that each time a more general system has been investigated, it has been possible to understand it, despite subtleties that have invariably emerged, in terms of the transition at point J.

4.1 Ellipsoidal particles

The intuition developed in Sec. II.A suggests that the coordination number at the jamming transition should be the isostatic number, which depends on the particle shape. Once rotational degrees of freedom are introduced, the isostatic number in three dimensions increases from $Z_{\rm iso} = 6$ to $Z_{\rm iso} = 10$ for ellipsoids of revolution, or spheroids. Thus, on the basis of the arguments in Sec. II.A., one might expect the number of contacts at the jamming transition, Z_c, to jump *discontinuously* from 6 to 10 as the shape of the particles is perturbed infinitesimally from a sphere to a spheroid. In fact, this is not what is observed (75, 76). The number of interacting neighbors at the transition increases *continuously* as the shape is varied (75–79).

This conundrum has recently been resolved (80). The isostatic number for spheres was obtained without considering the rotational degrees of freedom, which give rise to rotational soft modes that can be viewed as being localized on each sphere. As the spheres are deformed into spheroids, these soft modes are grad-

ually recruited into the vibrational spectrum at nonzero frequencies. At small distortions from a sphere, ε , the resulting predominantly-rotational modes form a new band that lies below the band of predominantly-translational modes found for spheres. The onset frequency of the upper band of modes scales as $\omega^\star \sim Z_c(\varepsilon) - 6$. This is exactly the same scaling that was observed for compression (see Eqs. 7 and 2), except that in this case the extra contacts are created not by compressing the particles together, but by deforming their shape. Similar results were found in two dimensions (81).

These results indicate that while changing the particle shape gives rise to new physics–in this case a new band of rotational modes–the scenario developed in Sec. II for point J is surprisingly robust. The scaling of the contact number at the jamming transition of ellipsoids can be predicted from the scaling of the contact number for spheres under compression. Thus, the singular case of spheres, like other singular points, controls a wide swath of behavior in its vicinity.

4.2 Frictional spheres

If the spheres have static friction, then in addition to the inter-particle normal forces, f_n, discussed so far, there can also be tangential forces, f_t, up to a threshold set by the usual friction law $f_t \leq \mu f_n$, where μ is the friction coefficient. The presence of tangential forces introduces torque balances conditions for a stable system, and changes the counting of the number of degrees of freedom. The result is that the isostatic number in the case of frictional particles is $Z^\mu_{\rm iso} = d + 1$ in d dimensions. Since $d+1 < 2d$ for $d \geq 2$, this means that at the jamming threshold, mechanically stable packings of frictional spheres can exist over a range of values

of Z, namely

$$d + 1 \leq Z_c \leq 2d. \tag{11}$$

In the case of frictionless particles, different mechanically stable packings created with different initial conditions have the same properties, described in Sec. II. A. Thus, the scaling of the elastic moduli, coordination number, and other quantities depends in the same way on the degree of compression above the jamming threshold, $\Delta\phi$, for different configurations. In the case of frictional particles, this is no longer the case because at the jamming threshold, different configurations can have different values of Z_c with different ϕ_c (16, 82–84). Nonetheless, it was found (84) that the static shear modulus obeys the expected scaling for point J with Z_c replaced with $Z_{\rm iso}^{\mu}$. From this result, one would therefore expect that only packings with $Z_c \approx Z_{\rm iso}^{\mu}$ would be marginal with many low-frequency vibrational modes as for frictionless spheres (84) (see Sec. II.B). Standard protocols produce mechanically stable packings with $Z_c \approx Z_{\rm iso}^{\mu}$ only for extremely high values of the friction coefficient, $\mu \to \infty$ (85,86). Thus, it would appear that most stable packings of frictional particles with more realistic values of μ would not resemble the marginally-jammed packings of frictionless particles.

This turns out not to be true, for the following reason (85, 87). Depending on how a frictional packing is prepared, there might be n_m contacts with tangential forces that are just at the Coulomb threshold, $f_t = \mu f_n$. Thus, f_t for these contacts are constrained and do not contribute to the number of degrees of freedom. The counting can therefore be generalized to (85, 87)

$$Z \geq (d + 1) + \frac{2n_m}{d} \equiv Z_{\rm iso}^{m}. \tag{12}$$

for mechanically stable packings. According to this criterion, all packings with Z close to $Z_{\rm iso}^{m}$ will be marginal, with many low-frequency excitations coming

from the slipping of tangential contacts that just exceed the Coulomb threshold. Thus, packings at *any* value of the friction coefficient μ can be prepared to be close to this generalized isostaticity criterion (87), which is approached at the lowest density that can typically be accessed for a given μ (86). Packings prepared very gently therefore tend to be marginal in this sense (87), and have properties very similar to those of frictionless sphere packings near the jamming threshold.

4.3 Long-ranged interactions

For long-ranged interactions, the number of interacting neighbors is technically infinite. For long-ranged repulsive interactions, point J–defined as the jamming threshold, below which no particles are interacting–must lie at zero density. For spheres with long-ranged attractions, point J does not even exist–it lies inside the vapor-liquid coexistence curve, at least for binary Lennard-Jones mixtures (9). Thus, long-ranged interactions have a non-perturbative effect on the jamming transition. It is possible, however, that the jamming transition might still influence behavior. For systems with interactions that decay with distance, for example, one would not expect weak interactions with distant particles to have a strong effect on the vibrational properties. Indeed, it was found that a variational approach could be used to predict the boson peak frequency, $\omega^\star$, even in systems with long-ranged interactions, and that the value of $\omega^\star$ is primarily determined by the strongest bonds in the system, whose number is not much larger than the isostatic value (88). Thus, the vibrational properties of such systems are similar to those of ideal spheres not far above point J.

4.4 Networks

Phillips (89) recognized long ago that isostaticity is important to many of the properties of network glasses (90–92). In such systems, bond-bending interactions can be viewed as giving rise to additional constraints, beyond those discussed in Sec. II. The proximity to the isostatic point can be tuned by varying the composition of a network glass; this gives rise to rich phase behavior and unusual properties near the isostatic point. Recently, Wyart (10, 93, 94) has extended the variational analysis introduced in Sec. II to examine the vibrational spectra of networks near isostaticity, such as rigid tetrahedra connected by flexible joints (95), used to model silica.

5 IMPLICATIONS FOR REAL GLASSFORMERS: OPEN QUESTIONS

Compared to other jamming systems such as foams, emulsions, colloidal suspensions of spherical particles and granular bead packings, real glassforming systems arguably resemble ideal spheres the least. The constituent molecules or atoms are not spherical, they have long-ranged attractions, and they may have 3-body interactions such as bond-bending interactions in network glasses. The work reviewed in the last section suggests that point J may shed light on the vibrational properties of glasses. In this section, we will discuss the connection of the properties of marginally-jammed sphere packings with the low- to intermediate-temperature properties of amorphous solids, and the possible connection of the jamming transition to the glass transition.

5.1 Jammed sphere packings and amorphous solids

We have gone on at some length to describe the new physics that is controlled by the critical nature of point J. These have included structural properties appearing in the pair distribution function $g(r)$ and the presence of a new class of normal mode excitations. In studying the properties of these excitations, it has become clear that they have much to tell us about the low-temperature properties of glasses. They produce a large excess number of excitations (known as the Boson peak) and they are poor transporters of energy. The onset frequency of the Boson peak in the density of vibrational states, $\omega^\star$, would show up as a peak in the heat capacity at temperature $T \approx \hbar\omega^\star$. Similarly, the small and constant energy diffusivity associated with the modes above $\omega^\star$ should give rise to a linear increase of the thermal conductivity above $T \approx \hbar\omega^\star$, crossing over to a constant at $T \approx \hbar\omega_{\max}$, where $\omega_{\max}$ marks the Debye frequency, or the upper limit of the vibrational spectrum (19).

Real amorphous solids universally exhibit this very same behavior in the intermediate temperature regime, from 1K to room temperature (96). In this regime, the thermal conductivity, $\kappa(T)$, has a plateau followed by a nearly-linear rise at higher T, crossing over to a constant; this behavior is in sharp contrast to that of crystalline materials in the same temperature range (97). In addition, the ratio $C(T)/T^3$ of the heat capacity to the expected T^3 dependence predicted by the Debye model for crystalline solids exhibits a characteristic peak, also known as a Boson peak (96, 98), which is not seen in crystals. However, the origin of the plateau in the thermal conductivity and the question of whether the plateau is related to the Boson peak in the heat capacity remain controversial.

In jammed sphere packings, it is clear that the Boson peak in the heat capacity

is tied to the onset of linear behavior in the thermal conductivity through the frequency $\omega^\star$. The fact that $\omega^\star$ is only weakly affected by long-ranged interactions (88) and also emerges in models of network glasses (93, 94) as well as in ellipsoid packings (80) suggests that it is a robust feature that may well appear in real glasses. Thus, the jamming scenario predicts that it is not a coincidence that the Boson peak in the heat capacity occurs in the same temperature range as the end of the plateau in the thermal conductivity.

This still leaves open the question of the origin of the apparently universal behavior of amorphous solids at low temperature. There, the heat capacity increases approximately linearly in T (96), instead of as T^3 as expected, while the thermal conductivity increases as T^2 instead of as T^3 as it does for crystals (99). It is believed that these features arise from the scattering of phonons from two-level systems (96, 100). However, two-level systems are not yet understood in physical terms.

The recent discovery (65, 71) that anharmonic effects in jammed sphere packings are very different from those in crystals may open new doors. The low-frequency modes of jammed systems are, by many measures, considerably more anharmonic than the high-frequency ones. The large anharmonicity coupled with the strong quasi-localization of low-frequency modes may give rise to the exciting possibility of local melting and concomitant dynamical heterogeneities (71, 101). It may be possible to identify two-level systems and shear transformation zones (102, 103). We suggest that this is one of the most exciting avenues to explore in the near future.

5.2 Point J and the glass transition

One question of current controversy is whether there is a connection of point J to the glass transition. There have been a number of papers that have recently suggested that the jamming and the glass transition are separate phenomena (50, 104). For example, Fig. 7(a) shows a scenario in which there is a true thermodynamic glass transition at nonzero T/p, labeled as K, which is clearly distinct from the line of J-points at $T/p = 0$. An alternate scenario is depicted in Fig. 7(b), in which there is no thermodynamic glass transition at nonzero T/p. Note that in both cases, it is assumed that the close-packed state is disordered, which is not the case for monodisperse or bidisperse systems.

Recent simulation results by Xu, et al. (68), discussed in Sec. III.B, demonstrate that it is still far from clear which of these two scenarios applies to finite-dimensional systems. The functional form of the collapse function for the relaxation time determines whether there is an intervening thermodynamic glass transition (if the function diverges at a finite value of T/p) or whether the relaxation in the vicinity of the jamming point is governed by the jamming transition itself (if the function diverges only at$T/p = 0$) (68). Equivalently, for hard spheres one may ask whether the relaxation time diverges when the pressure diverges or when it is finite (33,105). If it diverges at a finite pressure, then the glass transition and jamming transition are distinct; if it diverges at infinite pressure, then the only thermodynamic glass transition is the jamming transition.

The results of Ref. (68) show that it is not possible to determine which scenario is correct with the dynamical range available to simulations. Experiments on glassforming liquids cannot determine where the relaxation time diverges with 14 orders of magnitude of dynamic range, and simulations and experiments on

hard-sphere-like colloids can only probe about 5 decades. In addition, we have no fundamental understanding of the form of the equation of state or relaxation time scaling functions. Thus, this question seems unanswerable at the present time.

We must also ask what happens to the dynamics when we go beyond the ideal sphere model. For example, do attractive interactions completely disrupt the scaling scenario for the relaxation times that appear near point J for repulsive interactions? Recent studies (106) suggest that the density dependence of the relaxation time is very different for systems with attractions than for systems with only repulsions. Nevertheless, our experience with liquids (107) suggests that the physics can be dominated by repulsions. The understanding of the effect of attractions is an area of active research.

5.3 Conclusion

Jamming provides a fertile field for future research. It should be clear from this review that there are many parallels between phenomena observed in computer simulations of jammed sphere packings and those observed in amorphous systems existing in the laboratory. The parallels appear despite what must be admitted are the drastic idealizations used in the canonical model of jamming: a collection of frictionless spheres interacting via repulsive, finite-ranged, two-body potentials at zero temperature. Many issues still remain to be answered that focus on different aspects of the jamming scenario.

Over the last decade, most of the research on the jamming transition was on simulated systems where the interactions could be very tightly controlled, with the notable exception of experiments on emulsions and foams measuring the

scaling of elastic moduli (108, 109). Recently, however, a number of experiments have been performed that are capable of testing some of the predictions of the simulations. These include experiments that focus on structural features (66, 110–113), experiments on rheology near the jamming transition (114–116) and experiments on granular systems near the transition (110, 111, 117–119).

Moreover, a number of reports have recently come out of experiments that are designed to measure the distribution of low-frequency anomalous modes in colloidal samples that have densities that are adjusted to vary through the jamming transition (66, 120) (M. Gardel, unpublished). These experiments will be able to test whether the picture of the vibrational properties obtained from simulations on idealized spheres applies to real systems.

Our conclusions are highly optimistic. Recent discoveries in jammed particle packings have opened new doors into understanding how amorphous systems behave in general. A number of studies suggest that many properties of glasses may be governed by the proximity to a novel and unusual critical point that marks the jamming transition of frictionless spheres at zero temperature. This new physics is still being unraveled.

5.4 Acknowledgements

We have benefited from discussions with too many people to be listed here, but would particularly like to thank T. K. Haxton, C. S. O'Hern, J. M. Schwarz, L. E. Silbert, N. Xu, V. Vitelli, M. Wyart and Z. Zeravcic for stimulating collaborations. In addition, we thank the Kavli Institute for Theoretical Physics in Santa Barbara for hospitality at the inception of the field. We are grateful for funding from the Department of Energy via DE-FG02-05ER46199 (AJL) and DE-FG02-

03ER46088 (SRN) and the National Science Foundation MRSEC program via DMR-0520020 (AJL) and DMR-0820054 (SRN).

Literature Cited

1. Ediger MD, Austen, CA, Nagel SR. 1996. J. Phys. Chem. 100:13200
2. Debenedetti PG, Stillinger FH. 2001. Nature 410:259
3. Liu AJ, Nagel SR. 1998. Nature 396:21
4. Malandro DL, Lacks DJ. 1999. J. Chem. Phys. 110:4593
5. Maloney CE, Lemaitre A. 2006. Phys. Rev. E 74:016118
6. Maxwell JC. 1865. Phil. Mag. 27:294
7. Alexander S. 1998. Phys. Rep. 296:65
8. Moukarzel CF. 1998. Phys. Rev. Lett. 81:1634
9. O'Hern CS, Silbert LE, Liu AJ, Nagel SR. 2003. Phys. Rev. E 68:011306
10. Wyart M. 2005. Ann. Phys. Fr. 30:1
11. Durian DJ. 1995. Phys. Rev. Lett. 75:4780
12. O'Hern CS, Langer SA, Liu AJ, Nagel SR. 2002. Phys. Rev. Lett. 88:075507
13. Wyart M, Nagel SR, Witten TA. 2005. Europhys. Lett. 72:486
14. Wyart M, Silbert LE, Nagel SR, Witten TA. 2005. Phys. Rev. E 72:051306
15. Silbert LE, Liu AJ, Nagel SR. 2006. Phys. Rev. E 73:041304.
16. Silbert LE, Ertaş D, Grest GS, Halsey TC, Levine D. 2002. Phys. Rev. E 65:051307
17. Donev A, Torquato S, Stillinger FH. 2005. Phys. Rev. E 71:011105
18. Silbert LE, Liu AJ, Nagel SR. 2005. Phys. Rev. Lett. 95:098301
19. Vitelli V, Xu N, Wyart M, Liu AJ, Nagel SR. 2009. arXiv: 0908.2176
20. Xu N, Vitelli V, Wyart M, Liu AJ, Nagel SR. 2009. Phys. Rev. Lett.

102:038001

21. Wyart M. 2009. arXiv: 0909.2616
22. Drocco JA, Hastings MB, Olson Reichhardt CJ, Reichardt C. 2005. Phys. Rev. Lett. 95:088001
23. Olsson P, Teitel S. 2007. Phys. Rev. Lett. 99:178001
24. Kirkpatrick TR, Thirumalai D, Wolynes PG. 1989. Phys. Rev. A 40:1045
25. Souslov A, Liu AJ, Lubensky TC. 2009. Phys. Rev. Lett. 103:205503
26. Ellenbroek WG, Zeravcic Z, van Hecke M, van Saarloos W. 2009. Europhys. Lett. 87:34004
27. Mao X, , Xu N, Lubensky TC. 2009. arXiv:0907.2616
28. Kirkpatrick TR, Thirumalai D. 1987. Phys. Rev. Lett. 58:2091
29. Kirkpatrick TR, Thirumalai D. 1987. Phys. Rev. B 36:5388
30. Yin H, Chakraborty B. 2001. Phys. Rev. Lett. 86:2058
31. Toninelli C, Biroli G, Fisher DS. 2004. Phys. Rev. Lett. 92:185504
32. Biroli G, Bouchaud JP. 2004. Europhys. Lett. 67:21
33. Parisi G, Zamponi F. 2005. J. Chem. Phys. 123:144501
34. Chalupa J, Leath P, Reich GR. 1979. J. Phys. C 12:L31
35. Toninelli C, Biroli G, Fisher DS. 2004. Phys. Rev. Lett. 92:185504
36. Toninelli C, Biroli G, Fisher DS. 2005. J. Stat. Phys. 120:167
37. Toninelli C, Biroli G, Fisher DS. 2006. Phys. Rev. Lett. 96:035702
38. Toninelli C, Biroli G. 2007. J. Stat. Phys. 126:731
39. Jeng M, Schwarz JM. 2008. J. Stat. Phys. 131:575
40. Schwarz JM, Liu AJ, Chayes LQ. 2006. Europhys. Lett. 73:560 (2006).
41. Fredrickson GH, Andersen HC. 1984. Phys. Rev. Lett. 53:1244
42. Sellitto M, Biroli G, Toninelli C. 2005. Europhys. Lett. 69:496

43. Edwards SF, Oakeshott RBS. 1989. Physica A 157:1080

44. Blumenfeld R, Edwards SF. 2003. Phys. Rev. Lett. 90:114303

45. Blumenfeld R, Edwards SF. 2009. J. Phys. Chem. B 113:3981

46. Henkes S, O'Hern CS, Chakraborty B. 2007. Phys. Rev. Lett. 99:038002

47. Henkes S, Chakraborty B. 2009. Phys. Rev. E 79:061301

48. Henkes S, Chakraborty B. 2005. Phys. Rev. Lett. 95:098002

49. Torquato S, Stillinger FH. 2001. J. Phys. Chem. B 105:11849

50. Mari R, Krzakala F, Kurchan J. 2009. Phys. Rev. Lett. 103:025701

51. Chaudhuri P, Berthier L, Sastry S. 2009. arXiv:0910.0364

52. Feldman JL, Allen PB, Bickham SR. 1999. Phys. Rev. B 59:3551

53. Biswas R, Bouchard AM, Kamitakahara WA, Grest GS, Soukoulis CM. 1998. Phys. Rev. Lett. 60:2280

54. Bucheanau U, Galperin YM, Gurevich VL, Parshin DA, Ramos MA, Schober HR. 1992. Phys. Rev. B 46:2798

55. Buchenau U, Pecharroman C, Zorn R, Frick B. 1996. Phys. Rev. Lett. 77:659

56. Fabian J, Allen PB. 1997. Phys. Rev. Lett. 79:1885

57. R.Schober H, Ruocco G. 2004. Phil. Mag. 84:1361

58. Taraskin SN, Elliott SR. 1999. Phys. Rev. B 59:8572

59. Vainer YG, Naumov AV, Bauer M, Kador L. 2006. Phys. Rev. Lett. 97:185501

60. Silbert LE, Liu AJ, Nagel SR. 2009. Phys. Rev. E 79:021308

61. Kittel C. 1949. Phys. Rev. B 57:972

62. Soven P. 1969. Phys. Rev. 178:1136

63. Kirkpatrick S. 1973. Rev. Mod. Phys. 45:574

64. Garboczi EJ, Thorpe MF. 1985. Phys. Rev. Lett. 31:7276

65. Xu N, Vitelli V, Liu AJ, Nagel SR. 2009. arXiv: 0909.3701

66. Zhang Z, Xu N, Chen DTN, Yunker P, Alsayed AM, et al., 2009. Nature 459:230

67. Xu N. 2009. arXiv:0911.1576

68. Xu N, Haxton TK, Liu AJ, Nagel SR. 2009. Phys. Rev. Lett. 103:245701

69. Donev A, Stillinger FH, Torquato S. 2006. Phys. Rev. Lett. 96:225502

70. Brito C, Wyart M. 2007. Europhys. Lett. 99:149

71. Brito C, Wyart M. 2007. J. Stat. Mech. Theory - Exp 2007:L08003

72. Brito C, Wyart M. 2009. J. Chem. Phys. 131:024504

73. Ferguson A, Fisher B, Chakraborty B. 2004. Europhys. Lett. 66:277

74. Durian DJ. 1997. Phys. Rev. E 55:1739

75. Man W, Donev A, Stillinger FH, Sullivan MT, Russel WB, et al.. 2005. Phys. Rev. Lett. 94:198001

76. Donev A, Cisse I, Sachs D, Variano EA, Stillinger FH, et al. 2004. Science 303:990

77. Donev A, Connelly R, Stillinger FH, Torquato S. 2007. Phys. Rev. E 75:051304

78. Sacanna S, Rossi L, Wouterse A, Philipse AP. 2007. J. Phys. Cond. Matt. 19:6108

79. Wouterse A, Williams SR, Philipse AP. 2007. J. Phys. Cond. Matt. 19:6215

80. Zeravcic Z, Xu N, Liu AJ, Nagel SR, van Saarloos W. 2009. Europhys. Lett. 87:26001

81. Mailman M., Schreck, CF, O'Hern CS, Chakraborty B. 2009. Phys. Rev. Lett. 102:255501

82. Zhang HP, Makse HA. 2005. Phys. Rev. E 72:011301

83. Somfai E, Roux JN, Snoeijer JH, van Hecke M, van Saarloos W. 2005. Phys. Rev. E 72:021301

84. Somfai E, van Hecke M, Ellenbroek WG, Shundyak K, van Saarloos W. 2007. Phys. Rev. E 75:020301(R)

85. Shundyak K, van Hecke M, van Saarloos W. 2007. Phys. Rev. E 75:010301 (R)

86. Song C, Wang P, Makse HA. 2008. Nature 453:629

87. Henkes S, van Hecke M, van Saarloos W. 2009. arXiv:0907.3451

88. Xu N, Wyart M, Liu AJ, Nagel SR, 2007. Phys. Rev. Lett. 98:175502

89. Phillips JC. 1979. J. Non-Cryst. Sol. 34:153

90. Phillips JC, Thorpe MF. 1985. Sol. State Comm. 53:699

91. He H, Thorpe MF. 1985. Phys. Rev. Lett. 54:2107

92. Boolchand P, Lucovsky, G., Phillips JC, Thorpe MF. 2005. Phil. Mag. 85:3823.

93. Wyart M. 2009. Rigidity-based approach to the boson peak in amorphous solids: from sphere packing to amorphous silica. In Rigidity and Boolchand Intermediate Phases in Nanomaterials, 159–177. Bucarest, 2009, INOE Bucarest.

94. Wyart M, Liang H, Kabla A, Mahadevan L. 2008. Phys. Rev. Lett. 101:215501

95. Trachenko KO, Dove MT, Harris MJ, Heine V. 2000. J. Phys. Cond. Matt. 12:8041

96. Anderson AC. 1981. In Amorphous Solids, Low Temperature Properties, ed. Phillips WA. Berlin: Springer.

97. Cahill DG, Pohl RO. 1987. Phys. Rev. B 35:4067

98. Liu X, van Löhneysen H. 1996. Europhys. Lett. 8:617

99. Zeller RC, Pohl RO. 1971. Phys. Rev. B 4:2029

100. Anderson PW, Halperin BI, Varma CM. 1972. Philos. Mag. 25:1

101. Widmer-Cooper A, Perry H, Harrowell P, Reichman DR. 2009. Nature Phys. 4:711

102. Falk ML, Langer JS. 1998. Phys. Rev. E 57:7192

103. Langer JS. 2008. Phys. Rev. E 57:021502

104. Berthier L, Witten TA. 2009. Europhys. Lett. 86:10001

105. Berthier L, Witten TA. 2009. Phys. Rev. E 80:021502

106. Berthier L, Tarjus G. 2009. Phys. Rev. Lett. 103:170601

107. Weeks JD, Chandler D, Andersen HC. 1971. J. Chem. Phys. 54: 5237

108. Mason TG, Bibette J, Weitz DA. 1995. Phys. Rev. Lett. 75:2051

109. Saint-Jalmes A, Durian DJ. 1999. J. Rheol. 43:1411

110. Abate AR, Durian DJ. 2006. Phys. Rev. E 74:031308

111. Keys AS, Abate AR, Glotzer SC, Durian DJ. 2007. Nature Phys. 3:260 (2007).

112. Cheng X. 2009. arXiv: 0905.2788.

113. Clusel M, Corwin EI, Alexander, Siemens ON, Brujic J. 2009. Nature 460:611

114. Katgert G, Moebius ME, van Hecke M. 2009. Phys. Rev. E 101:058301

115. Katgert G, Latka A, Moebius ME, van Hecke M. 2009. Phys. Rev. E 79:066318

116. Nordstrom K, Durian DJ, Gollub J. 2009. Bull. Am. Phys. Soc., March Meeting, X9.4.

117. Majmudar T, Sperl M, Luding S, Behringer R. 2007. Phys. Rev. Lett.

98:058001

118. Behringer RP, Bi D, Chakraborty B, Henkes S, Hartley RR. 2008. Phys. Rev. Lett. 101:268301

119. Bonneau L, Andreotti B, Clément E. 2008. Phys. Rev. Lett. 101:118001

120. Ghosh A, Chikkadi V, Schall P, Kurchan J, Bonn D. 2009. arXiv: 0910.3231.

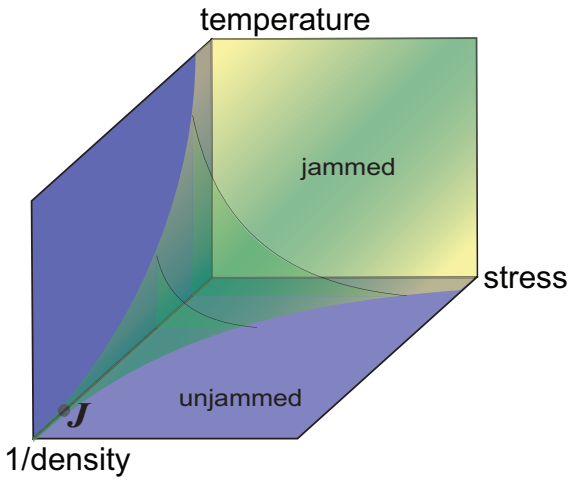

Figure 1: Jamming phase diagram. Outside the shaded region, at high temperature, T, applied shear stress, Σ and high inverse density, $1/\phi$, the system is unjammed and can flow; inside the shaded region the system is jammed. The point "J" marks the jamming transition for ideal spheres at zero temperature and applied stress.

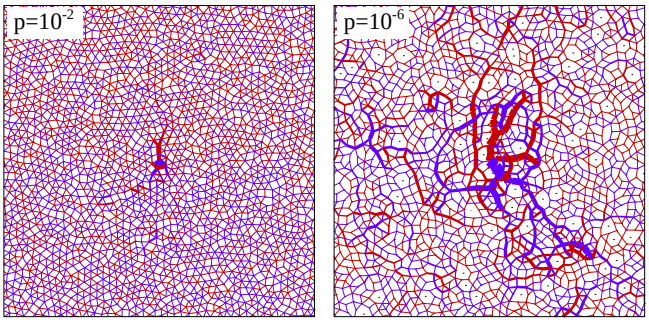

Figure 2: Response to a force loaded at the center with blue (red) lines indicating an increase (decrease) on each bond. The thickness of each line is proportional to the change in force. Left: system at a higher compression with pressure $p = 10^{-2}$; right: system close to the transition with $p = 10^{-6}$. Forces are affected to a distance that scales as $\ell^\star$.

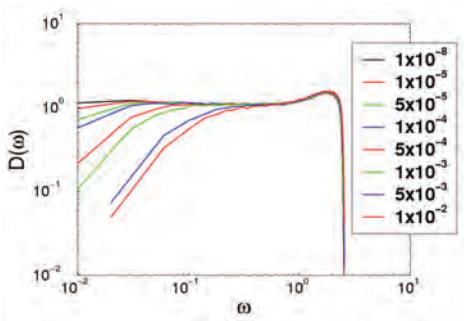

Figure 3: Density of vibrational states for three-dimensional ideal sphere packings with harmonic repulsions at various compressions, $\Delta\phi$ (18). The density of states approaches a constant as $\Delta\phi \to 0$.

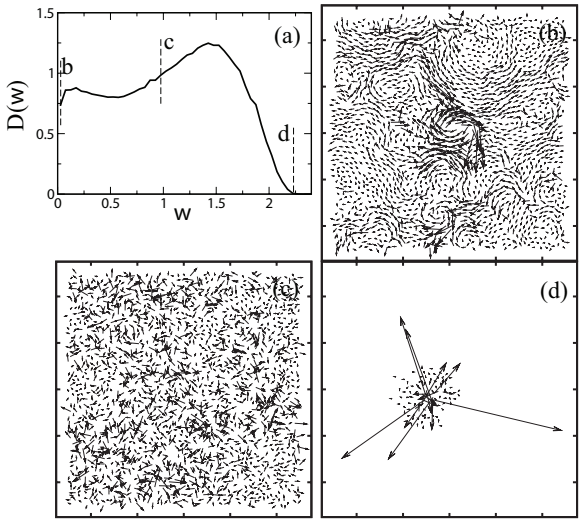

Figure 4: Vibrational modes of a $d = 2$ packing of $N = 2000$ particles at $\Delta\phi = 10^{-4}$. (a) The density of states, with vertical lines indicating frequencies of the modes in (b-d). (b) a quasi-localized mode, (c) an extended anomalous mode and (d) a localized mode at high frequency.

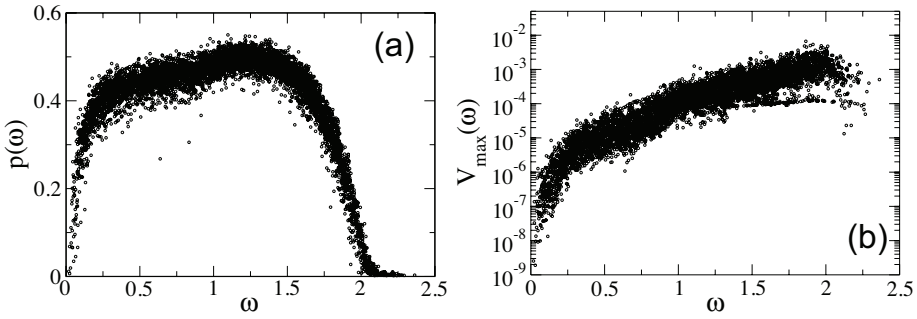

Figure 5: (a) Participation ratio $p(\omega_i) = \frac{\left(\sum_n |\mathbf{e}_{n,i}|^2\right)^2}{N \sum_n |\mathbf{e}_{n,i}|^4}$ of the vibrational modes, where $\mathbf{e}_{n,i}$ is the displacement of particle n in mode i. (b) energy barrier $V_{\max}$ encountered along each mode before falling into another energy basin. Data are for a configuration of $N = 1000$ particles at $\Delta\phi = 0.1$. The modes with the smallest participation ratios have the lowest barriers to rearrangements.

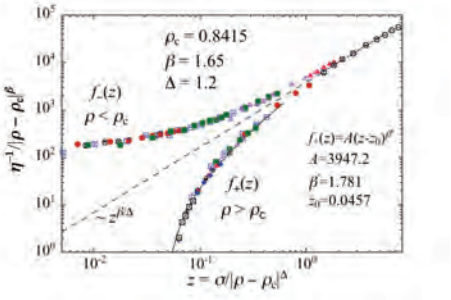

Figure 6: Scaling plot showing inverse viscosity scaled by $\Delta\phi^\beta$ vs. shear stress rescaled by $\Delta\phi^\Delta$. The two branches of the scaling function, corresponding to $\phi < \phi_c$ and $\phi > \phi_c$, respectively, are collapsed by the same exponents, consistent with behavior near an ordinary critical point. After Ref. (23).

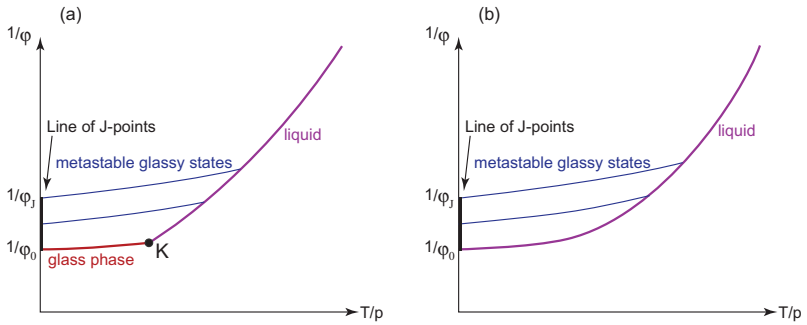

Figure 7: A "jamming state diagram" in the plane of inverse packing fraction, $1/\phi$, and the ratio of temperature to pressure, T/p. At zero temperature, different trajectories (blue lines) corresponding to different cooling or compression rates lead to $T = 0$ states with different ϕ_c. The fastest cooling rate (highest blue line) leads to the lowest critical packing fraction. (a) Diagram constructed for mean-field "random first-order models" that have a thermodynamic glass transition labeled by K that is distinct from the line of J-points. After Ref. (50). (b) Alternate version of the diagram for systems that do not have a thermodynamic glass transition but have a close-packed state that is disordered.